Cataclysmic variables from a ROSAT/2MASS selection I: Four new intermediate polars

B. T. Gänsicke[1], T.R. Marsh[1], A. Edge[2], P. Rodríguez-Gil[1,3], D. Steeghs[4],
S. Araujo-Betancor[5], E. Harlaftis[6], O. Giannakis[7], S. Pyrzas[8], L. Morales-Rueda[9],
A. Aungwerojwit[1]

[1] *Department of Physics, University of Warwick, Coventry CV4 7AL, UK*
[2] *Department of Physics, University of Durham, South Road, Durham DH1 3LE, UK*
[3] *Instituto de Astrofísica de Canarias, 38200 La Laguna, Tenerife, Spain*
[4] *Harvard-Smithsonian Center for Astrophysics, 60 Garden Street, MS-67, Cambridge, MA 02138, USA*
[5] *Space Telescope Science Institute, 3700 San Martin Drive, Baltimore, MD21218, USA*
[6] *Institute of Space Applications and Remote Sensing, National Observatory of Athens, P.O. Box 20048, Athens 11810, Greece*
[7] *Institute of Astronomy, National Observatory of Athens, P.O. Box 20048, Athens 11810, Greece*
[8] *Department of Physics, Section of Astrophysics, Astronomy & Mechanics, University of Thessaloniki, 541 24 Thessaloniki, Greece*
[9] *Department of Astrophysics, University of Nijmegen, PO Box 9010, 6500GL, Nijmegen, The Netherlands*

ABSTRACT

We report the first results from a new search for cataclysmic variables (CVs) using a combined X-ray (ROSAT) / infrared (2MASS) target selection that discriminates against background AGN. Identification spectra were obtained at the Isaac Newton Telescope for a total of 174 targets, leading to the discovery of 12 new CVs. Initially devised to find short-period low-mass-transfer CVs, this selection scheme has been very successful in identifying new intermediate polars. Photometric and spectroscopic follow-up observations identify four of the new CVs as intermediate polars: 1RXS J063631.9+353537 ($P_{\rm orb} \simeq 201\,{\rm min}$, $P_{\rm spin} = 1008.3408\,{\rm s}$ or $930.5829\,{\rm s}$), 1RXS J070407.9+262501 ($P_{\rm orb} \simeq 250\,{\rm min}$, $P_{\rm spin} = 480.708\,{\rm s}$), 1RXS J173021.5−055933 ($P_{\rm orb} = 925.27\,{\rm min}$, $P_{\rm spin} = 128.0\,{\rm s}$), and 1RXS J180340.0+401214 ($P_{\rm orb} = 160.21\,{\rm min}$, $P_{\rm spin} = 1520.51\,{\rm s}$). RX J1730, also a moderately bright hard X-ray source in the INTEGRAL/IBIS Galactic plane survey, resembles the enigmatic AE Aqr. It is likely that its white dwarf is not rotating at the spin equilibrium period, and the system may represent a short-lived phase in CV evolution.

Key words: accretion, accretion discs – binaries: close – novae, cataclysmic variables

1 INTRODUCTION

The evolution of cataclysmic variable stars (CVs) is driven by the need for the mass-donor stars to fill their Roche lobes. This is ensured by angular momentum loss (AML), through gravitational wave radiation and magnetic braking via a stellar wind, which gradually decreases the binary orbital period $P_{\rm orb}$. The standard theory of CV evolution assumes that magnetic braking ceases once the systems reach $P_{\rm orb} \simeq 3\,{\rm h}$ (e.g. Rappaport et al. 1983). With gravitational wave radiation being a much less efficient AML mechanism than magnetic braking, CVs with $P_{\rm orb} < 3\,{\rm h}$ have much lower mass transfer rates and longer evolution time scales than those with $P_{\rm orb} > 3\,{\rm h}$ (Kolb & Stehle 1996). Initially the mass donor shrinks in response to mass loss causing the orbital period to decrease. Eventually the mass donor becomes so low in mass ($< 0.08\,{\rm M_\odot}$) that fusion dies out and the star evolves towards a degenerate state. Its radius then starts to increase upon mass loss, leading to an increase

in the orbital period of the CV (Paczyński & Sienkiewicz 1983). Up to this point the decreasing period is compensated by the reduced mass of the donor bringing about a near-constant mass loss rate. After the period minimum (observationally found near 80 min) however, the simultaneous reduction in the mass of the donor and the increase in orbital period act to reduce AML resulting in a precipitous drop in the mass loss rate, and a further slowing of the CV's evolution. Consequently, the vast majority ($\sim 99\%$) should have periods $< 2\,{\rm h}$, and a large fraction of all CVs ($\sim 70\%$) should have passed through the period minimum (Kolb 1993; Howell et al. 1997).

The apparent lack of observed short-period CVs in general and "post-period-bounce" CVs in particlar is a major embarrassment for our understanding of compact binary evolution (e.g. Gänsicke et al. 2002b). Selection effects are an obvious and generally welcomed explanation for this discrepancy – about half of all known
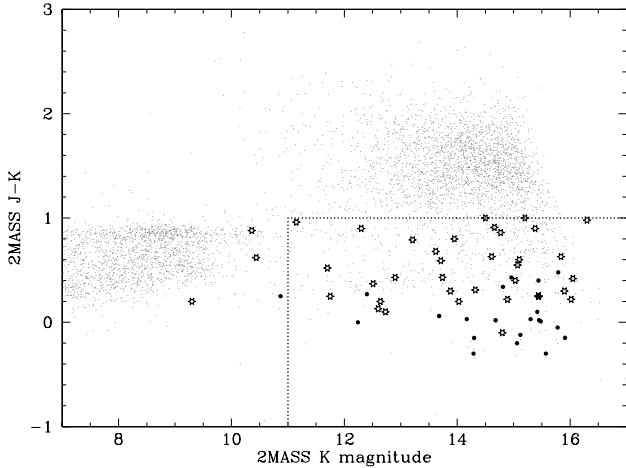
Figure 1. The 2MASS "magnitude-colour" diagram of stellar (point-like) sources from the ROSAT All Sky Survey with $|b| > 5°$ showing how infrared colours distinguish CVs and white dwarfs from other sources. Bright stars appear towards the left, while AGN appear in the upper-right. Known white dwarfs are marked black dots, known CVs by stars. There are 399 objects in the region $K > 11$, $J - K < 1.0$ designed to avoid the bright stars and AGN. This drops to 300 applying $R < 17$. About 50 of these are known leaving 250 unidentified targets.

CVs have been found because of strong variability, i.e. displaying outbursts (Gänsicke 2004). As the absolute magnitudes of CVs during outburst are a function of their orbital period, but *not* their mean mass transfer rate (Warner 1987), there is no obvious reason why post-period-bounce systems should not be found unless they very rarely or never go into outburst. Observationally, a number of systems are known that have very infrequent outbursts (e.g. WZ Sge, GW Lib, or LL And), or have had no observed outbursts (e.g. BW Scl, GD 552, HS 2331+3905, or GP Com). In fact, disc instability theory predicts that outburst activity may cease completely below a certain mass transfer rate (Meyer-Hofmeister et al. 1998). Thus, if the predicted large number of short-period low-mass-transfer CVs exists, they must be discovered by other means than variability. Spectroscopic surveys have demonstrated the ability to find such objects [the Hamburg Quasar Survey (Gänsicke et al. 2002b), the Sloan Digital Sky Survey (Szkody et al. 2005 and references therein), and the 2dF Quasar Survey (Marsh et al. 2002)], but the number of new short orbital period CVs discovered in this way also falls short of the predicted numbers. We have therefore initiated a new search for CVs based on one apparently common feature of low-mass-transfer systems: X-ray emission – of the six systems named above, WZ Sge, BW Scl, GD 552, and GP Com are noticeable X-ray sources (Voges et al. 1999), indeed, BW Scl was discovered in X-rays (= RX J2353.0-3852, Abbott et al. 1997). Here we report the first results from this search – the discovery of four new intermediate polars (IPs).

2   TARGET SELECTION

X-ray identification work has led to the discovery of various CVs not found by any other method (e.g. Schwope et al. 2002) and the ROSAT All-Sky Survey (RASS, Voges et al. 1999) still contains a large number of optically unidentified sources, particularly at intermediate Galactic latitudes ($5 < |b| < 30°$). The identification of CVs is complicated by the fact that they are rare and have sim-

ilar optical magnitudes and colours to the more numerous AGN. However, when near-infrared photometry from 2MASS is also considered there is a clear discrimination between the bulk of the AGN and CVs or white dwarfs (Fig. 1). We have drawn the X-ray sources for this project from the ROSAT Bright Source Catalogue (Voges et al. 1999), limiting the selection to count rates from 0.05 to 0.2 cts s^{-1}, a regime not systematically explored to date. There are over 10 000 such sources, but applying limitations on galactic latitude ($|b| > 5°$) to avoid confusion, infrared colours ($J - K < 1$ consistent with galactic sources) and infrared magnitude ($K > 11$ to exclude the majority of coronal stellar sources) leaves 399 sources. This drops to 300 with the additional restriction of $R < 17$ to allow identitifcation work with 2 m class telescopes. Since some 50 of these are known objects, mainly CVs or white dwarfs, 250 unidentified targets remain.

3   OBSERVATIONS: SPECTROSCOPY

Identification spectroscopy of the target sample and time-resolved follow-up spectroscopy of newly identified CVs was obtained with four different telescopes. A brief account of the used instrumentation and the data reduction procedures is given below.

3.1   Isaac Newton Telescope identification spectroscopy

The initial identification spectroscopy of ROSAT/2MASS CV candidate targets was carried out with the Intermediate Dispersion Spectrograph (IDS) on the Isaac Newton Telescope (INT), located at the Observatorio del Roque de los Muchachos on La Palma during 7 nights in August 2002 and 7 nights in March 2003 (Table 1). The spectra were obtained using the R400V grating on the 235 mm camera in conjunction with a 1.6 ″slit and an 4k pixel wide EEV CCD, resulting in a spectral coverage of $3900 - 7900$ Å at a resolution of $\simeq 3.5$ Å at the central wavelength. Standard data reduction (de-biasing, flat-fielding, optimal extraction, wavelength & flux calibration) was done using `Figaro` within the `STARLINK` suite and the `Pamela/Molly` packages.

While the 2002 run was done under nearly perfect conditions, the 2003 observations were seriously affected by bad weather, resulting in a number of candidates not being observed. Total of 174 targets were observed, leading to the discovery of 12 new CVs, including 1RXS J063631.9+353537, 1RXS J070407.9+262501, 1RXS J173021.5-055933, and 1RXS J180340.0+401214 (henceforth RX J0636, RX J0704, RX J1730, and RX J1803), which are discussed in this paper). The remaining new CVs as well as a list of all ROSAT source identifications will be published elsewhere. Coordinates, X-ray, optical and infrared properties of the four systems are given in Table 2, finding charts are shown in Fig. 3. The INT/IDS identification spectra of RX J0636, RX J0704, RX J1730 and RX J1803 all display Balmer and helium emission lines (Fig. 2), identifying them as CVs. The moderate to strong He II λ 4686 emission detected in their spectra indicates the presence of high-energy photons in these systems, typically a signature of magnetic CVs, high-mass-transfer novalike variables and post-novae. RX J0636, RX J0704 and RX J1730 have an equivalent width ratio He II λ 4686/Hβ > 0.5 (Table 2), which strongly suggests a magnetic nature of these systems. All three systems were confirmed to be magnetic CVs indeed by the detection of coherent short-period optical variability, the hallmark of IPs. RX J1803 has a relatively low He II λ 4686/Hβ ratio for being a magnetic system, but our photometry clearly identifies this object as an IP as well.
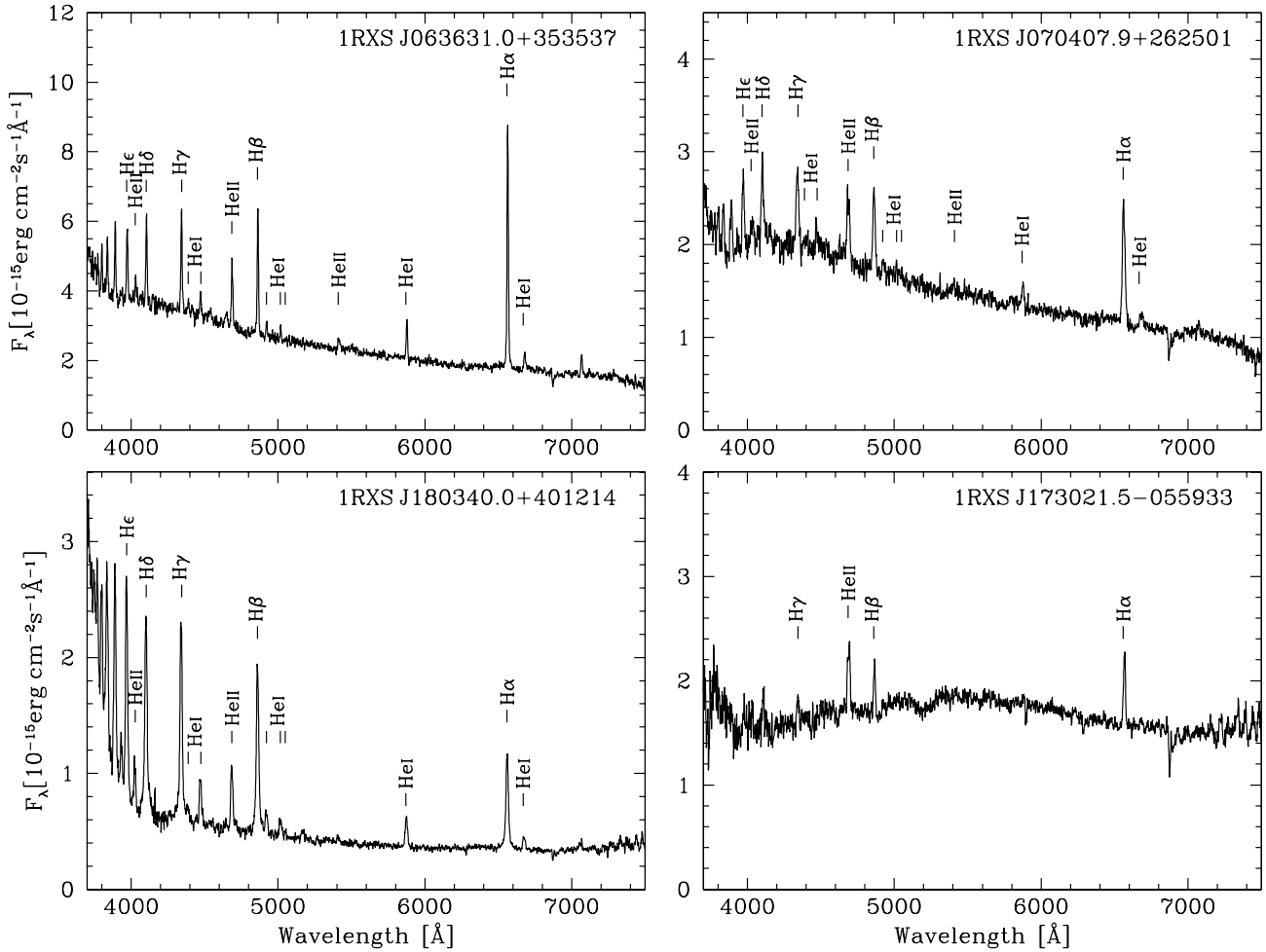
Figure 2. INT/IDS identification spectra of RX J0636, RX J0704, RX J1730, and RX J1803. The spectra have been smoothed with a 3-point boxcar.

3.2 Isaac Newton Telescope follow-up spectroscopy

Time-resolved follow-up spectroscopy of RX J1730 and RX J1803 was obtained at the INT in April/May 2003 using the R632V grating on the 235 mm camera with a 1.5″slit, covering the range $4640 - 6980$ Å with a spectral resolution of $\simeq 2$ Å (Table 1). Arc lamp calibration exposures were interleaved after every three object spectra to account for the flexure of the instrument. The follow-up spectra were processed in a standard fashion as described above using the long-slit reduction packages within IRAF[1]. The dispersion solutions were calculated by fitting a low-order polynomial to the arc data, and the pixel-to-wavelength relation for the target spectra were obtained from interpolating between the bracketing arc lamp exposures.

3.3 Calar Alto 2.2 m

Additional time-resolved spectroscopy of RXJ 1730, RXJ 1803, and RX J0704 was obtained at the Calar Alto 2.2 m telescope in April–June 2003 and in February 2005 using the Calar Alto Faint Object Spectrograph (CAFOS) equipped with the standard 2k × 2k

pixel SITe CCD and the G-100 grating. Using a 1.2″slit the observations covered the range $4240 - 8300$ Å at a resolution of ~ 4.1 Å (Table 1). Regular arc lamp exposures were taken to ensure an accurate wavelength calibration. The reduction of the CAFOS data was carried out using FIGARO, PAMELA & MOLLY as described in Sect. 3.1.

3.4 Magellan

RXJ 1730 was also observed with the B&C spectrograph on the 6.5 m Magellan-Clay telescope at Las Campanas Observatory in June 2003 under excellent seeing conditions (0.5–0.8″). The 600 grating blazed at 5000Å in conjunction with a 0.85″long-slit provided a wavelength coverage of 3890–7075Å at 1.55 Å/pixel on a 2048 × 515 Marconi CCD detector. The 58 target exposures (Table 1) were reduced and calibrated using the recipe described in Sect. 3.1 using regular arc lamp exposures and nightly observations of the spectrophotometric flux standard LTT9239.

3.5 William Herschel Telescope

Time-resolved spectroscopy of RXJ 0636 was carried out with the 4 m William Herschel Telescope (WHT) on La Palma in January

[1] IRAF is distributed by the National Optical Astronomy Observatories.

Table 1. Log of the observations

Date	UT	Obs	Filter/Grism	Exp.	Frames
1RXS J063631.9+353537					
2003 Mar 17	21:22	INT	R400V	900	1
2004 Oct 21	02:42 – 03:33	KY	clear	30	195
2004 Oct 22	00:07 – 03:43	KY	clear	20	510
2004 Oct 22	23:46 – 03:50	KY	clear	20	317
2004 Oct 23	23:12 – 00:37	KY	clear	20	187
2005 Jan 02	00:25 – 05:42	WHT	R600B/R316R	930	20
2005 Feb 21	20:46 – 00:52	KY	clear	45	254
2005 Feb 23	17:46 – 01:43	KY	clear	45	484
2005 Feb 24	17:16 – 22:17	KY	clear	45	352
2005 Mar 03	17:55 – 23:53	KY	clear	45	342
1RXS J070407.9+26250					
2003 Mar 18	21:16	INT	R400V	1800	1
2004 Dec 07	02:32 – 04:43	KY	clear	45	144
2005 Jan 02	00:30 – 06:49	INT	clear	60	254
2005 Jan 05	23:57 – 05:27	TNG	clear	30	511
2005 Feb 11	21:52 – 02:49	CA22	G100	600	21
1RXS J173021.5-055933					
2002 Aug 22	22:49	INT	R400V	900	1
2003 Apr 10	03:00 – 05:07	INT	???	1500	6
2003 Apr 11	03:29 – 05:16	INT	???	1500	5
2003 Apr 13	02:27 – 05:11	INT	???	1500	7
2003 Apr 22	03:29 – 04:22	INT	R632V	600	6
2003 Apr 26	03:29 – 04:22	INT	R632V	600	6
2003 Apr 27	04:26 – 05:19	INT	R632V	600	6
2003 May 10	01:09 – 05:41	JKT	*R*	30	339
2003 May 21	00:33 – 04:23	JKT	*R*	15–60	331
2003 May 20	01:49 – 01:59	INT	R632V	600	2
2003 Jun 21	23:44 – 02:40	CA22	G100	600	15
2003 Jun 22	23:21 – 03:06	CA22	G100	600	15
2003 Jun 23	05:11 – 07:55	MAG	G500/5000	120	27
2003 Jun 24	03:32 – 08:15	MAG	G500/5000	120	15
2003 Jun 25	02:39 – 03:15	MAG	G500/5000	120	16
2003 Jul 07	21:51 – 03:12	OGS	clear	20	631
2003 Jul 08	21:53 – 03:17	OGS	clear	10	1030
2003 Jul 09	21:31 – 22:31	OGS	*I*	25	112
2003 Jul 09	22:41 – 23:41	OGS	*R*	25	113
2003 Jul 09	23:52 – 00:51	OGS	*V*	30	95
2003 Jul 14	21:16 – 02:09	OGS	clear	15	777
2003 Jul 15	21:14 – 02:01	OGS	clear	10	1001
2003 Jul 16	21:30 – 03:23	OGS	clear	12	765
1RXS J180340.0+401214					
2002 Aug 21	21:27	INT	R400V	1800	1
2002 Aug 28	23:26	INT	R400V	1800	1
2003 Apr 23	04:41 – 05:34	INT	R632V	600	6
2003 Apr 25	04:39 – 05:42	INT	R632V	600	7
2003 Apr 29	02:55 – 03:59	CA22	G100	600	6
2003 May 02	03:46 – 04:20	CA22	G100	600	6
2003 May 19	04:15 – 05:08	INT	R632V	600	6
2003 May 20	04:24 – 05:17	INT	R632V	600	6
2003 May 21	22:41 – 04:13	JKT	*V*	80–100	186
2003 Jun 27	02:19 – 03:57	CA22	G100	600	9
2003 Jun 28	01:45 – 03:57	CA22	G100	600	12
2003 Aug 15	18:26 – 22:49	KY	clear	30	450
2003 Aug 16	18:30 – 23:02	KY	clear	30	498
2003 Aug 17	18:13 – 21:51	KY	clear	30	400
2003 Aug 18	18:08 – 22:18	KY	clear	30	440
2003 Aug 19	18:17 – 21:55	KY	clear	30	400

2005, using the ISIS double-arm spectrograph with the R600B grating and a 4k×2k pixel EEV detector in the blue and the R316R grating and a 4.5k×2k pixel Marconi detector in the red. Both arms were operated with a 1.2″slit, resulting in a spectral resolution of $\simeq 0.9$ Å covering the ranges $3600 - 5000$ Å and $6100 - 8900$ Å. Arc lamp and flat-field exposures were taken at regular intervals to ensure an accurate wavelength calibration and correct for CCD fringing in the red arm. The reduction of the WHT spectroscopy was done using FIGARO, PAMELA & MOLLY as described in Sect. 3.1.

4   OBSERVATIONS: PHOTOMETRY

Whereas the INT/IDS spectroscopy suggested a possible magnetic CV nature for all four systems (Sect. 3.1), the identification and confirmation of the IP nature of RX J0636, RX J0704, RX J1730 and RX J1803 has been derived from CCD time series obtained at four different telescopes. For all photometric data, instumental magnitudes of the target and two comparison stars (labelled 'C1' and 'C2' in Fig. 3) were extracted from the images, and differential light curves computed with respect to the comparison star 'C1'. Constant brightness of the primary comparison star and changes in the observing conditions were checked by inspecting the differential light curves 'C1'–'C2'. The details on the adopted comparison stars are given in Table 3. A brief description of the instrumentation at the different telescopes and the data reduction procedures is given below.

4.1   Kryoneri

Filterless CCD photometry of RX J0636, RX J0704, and RX J1730 was obtained at Kryoneri Observatory with the 1.2 m telescope using a Photometrics SI-502 516×516 pixel camera (Table 1). The images were de-biased, dark-current-subtracted, and flat-fielded within MIDAS and aperture photometry was performed using the SEXTRACTOR (Bertin & Arnouts 1996). A full account of the employed reduction pipeline is given by Gänsicke et al. (2004).

4.2   Jacobus Kapteyn Telescope

The 1.0 m Jacobus Kapteyn Telescope (JKT) on La Palma was used in May 2003 to obtain *R*-band photometry of RX J1730 and *V*-band photometry of RX J1803 using a SITe $2k \times 2k$ pixel CCD (Table 1). The reduction was carried out as described in Sect. 4.1.

4.3   Isaac Newton Telescope

The Wide Field Camera (WFC), an array of 4 EEV $2k \times 4k$ pixel CCDs, was used on the INT in January 2005 to obtain filterless photometry of RX J0704. The read-out time of the WFC is 42 s, resulting in a somewhat increased granularity of the observed light curves. The data were processed in an analogous way as described in Sect. 4.1.

4.4   Telescope Nazionale Galileo

We obtained g' CCD photometry of RX J0704 on the 3.6 m Telescopio Nazionale Galileo (TNG), located at the Observatorio del Roque de los Muchachos on La Palma, in January 2005 (Table 1). We used DOLORES equipped with a Loral $2k \times 2k$ pixel CCD. The reduction was carried out as described in Sect. 4.1.

Table 2. X-ray, optical and infrared properties of the four new CVs.

System	RA (2000)	Dec (2000)	PSPC 10^{-2}cts s^{-1}	HR1	HR2	He II Å	Hβ Å	Hα Å	B mag	R mag	J mag	H mag	K mag
1RXS J063631.9+353537	06 36 32.55	+35 35 43.3	5.0 ± 1.4	0.71 ± 0.25	0.33 ± 0.29	8	16	47	15.7	15.9	15.4	15.2	15.1
1RXS J070407.9+262501	07 04 08.67	+26 25 10.9	19.4 ± 3.3	-0.40 ± 0.14	0.55 ± 0.26	9	11	24	16.7	16.3	16.4	16.4	16.1
1RXS J173021.5-055933	17 30 21.90	-05 59 32.1	58.2 ± 4.1	0.86 ± 0.03	-0.05 ± 0.07	8	4	8	16.3	15.4	14.4	13.9	13.6
1RXS J180340.0+401214	18 03 39.67	+40 12 20.6	17.5 ± 1.5	-0.18 ± 0.08	-0.02 ± 0.12	18	66	52	18.0	17.1	15.2	14.8	14.4

Notes. The coordinates and the B and R magnitudes were taken from the USNO-B catalog (Monet et al. 2003), the ROSAT PSPC count rates and hardness ratios HR1 and HR2 have been obtained from the ROSAT All Sky Survey Bright Source Catalogue (Voges et al. 1999), the Hα, Hβ and He II equivalent widths were measured from the INT/IDS identification spectra (Fig. 2) using the `integrate/line` task in MIDAS, and the J, H, and K magnituds were taken from the 2MASS All Sky Survey.
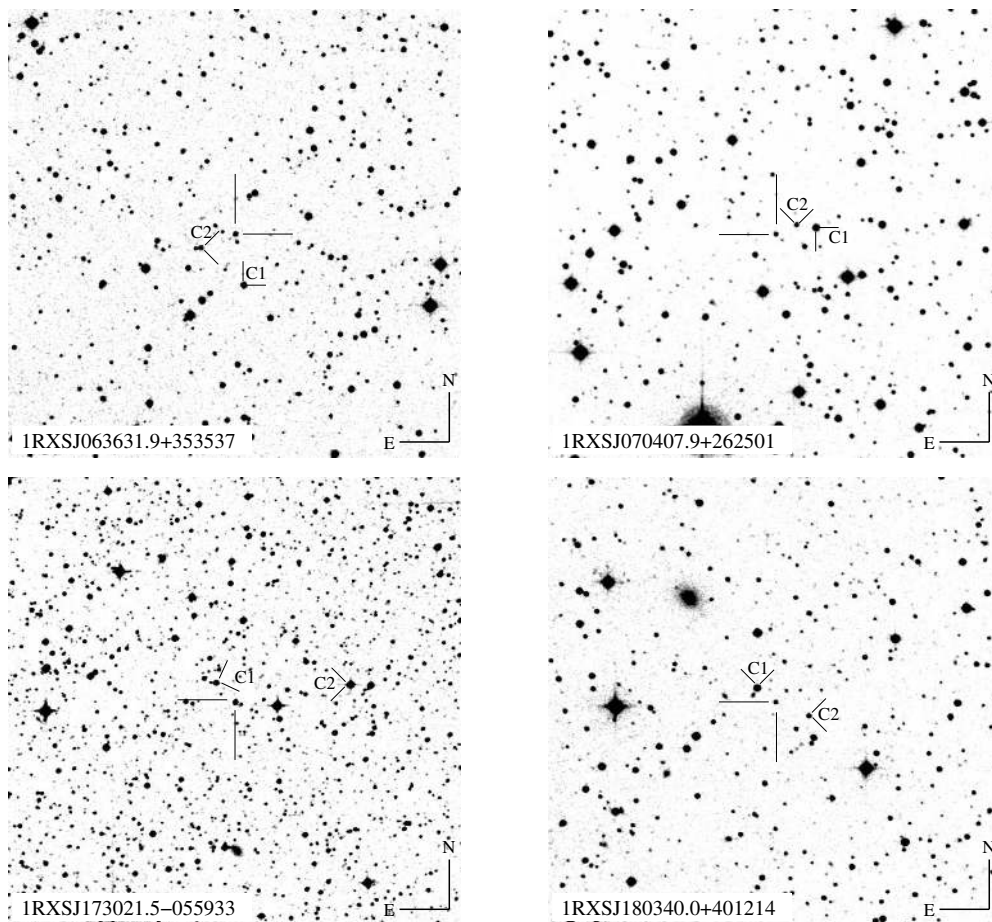
Figure 3. $10' \times 10'$ finding charts of RX J0636, RX J0704, RX J1730, and RX J1803 obtained from the Digitized Sky Survey 2. Primary and secondary comparison stars for the CCD photometry are labelled 'C1' and 'C2', see Table 3 for details.

4.5 Optical Ground Station

The 1 m Optical Ground Station (OGS) located at the Observatorio del Teide on Tenerife was used in July 2003 to obtain filterless and V-, R-, and I-band photometry of RX J1730. The telescope was equipped with a Thomson 1k × 1k pixel CCD camera. The images were bias and flat-field corrected and aligned within IRAF. Instrumental magnitudes of the CV and the comparison star 'C1' were then extracted using the point spread function (PSF) photometry tasks package within IRAF.

5 ANALYSIS AND RESULTS

5.1 1RXS J063631.9+353537

The INT/IDS identification spectrum of RX J0636 (Fig. 2) is characterised by narrow Balmer and He emission lines superimposed on a blue continuum. The detection of relatively strong He II λ 4686 suggests a potential magnetic CV nature for this system. No obvious signature of the donor star is detected in the spectrum.

Table 3. Comparison stars used for the differential CCD photometry.

| System	USNO reference	B	R
RX J0636	1200_04969236	15.7	15.9
'C1'	1200_04968961	15.7	14.5
'C2'	1200_04968814	17.3	16.0
RX J0704	1125_04825852	16.3	16.2
'C1'	1125_04824886	16.1	14.2
'C2'	1125_04825384	18.0	16.2
RX J1730	0825_10606993	16.5	15.8
'C1'	0825_10607901	16.9	15.5
'C2'	0825_10601801	15.8	13.7
RX J1803	1275_09738647	17.3	17.2
'C1'	1275_09739056	15.1	14.1
'C2'	1275_09737883	17.9	16.7
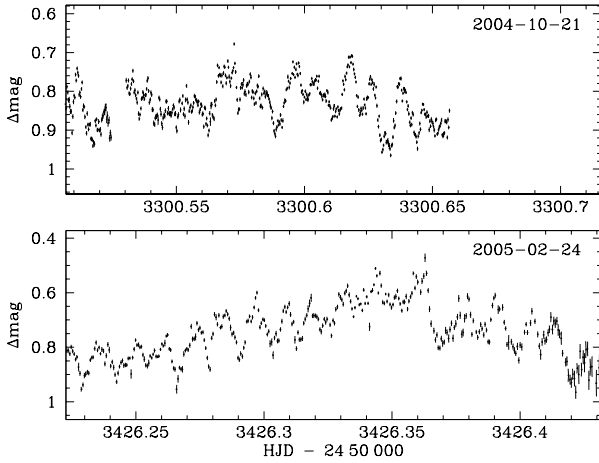
Figure 4. Sample light curves of RX J0636 obtained with the 1.2 m Kryoneri telescope.

5.1.1 Photometry

The CCD photometry of RX J0636 obtained at Kryoneri observatory in October 2004 and February/March 2005 (Table 1, Fig. 4) displays substantial variability on time scales of ~ 15 min, superimposed on longer-term modulations. Figure 5 shows a Scargle (1982) periodogram computed from the combined photometric data, using the MIDAS/TSA context. The suspected presence of a coherent short-period modulation is confirmed by the detection of relatively strong signal at $\simeq 85.7\,\mathrm{d}^{-1}$, with a 1-day alias of nearly equal strength at $\simeq 84.7\,\mathrm{d}^{-1}$. A second cluster of signals peaks at $\simeq 92.9\,\mathrm{d}^{-1}$ and $\simeq 91.9\,\mathrm{d}^{-1}$. The periods corresponding to the highest peaks of each cluster of signals are 1008.3408(19)s and 930.5829(40)s, respectively, where the errors have been determined from fitting a sine wave to the photometric data. In order to facilitate an improvement in the accuracy of the spin period, we have fitted a sine wave with the period fixed to the best-value determined from the entire data set to each individual night of photometry, and report in Table 4 the times of spin maxima determed from these fits. Folding the photometric data over the 1008s period results in a quasi-sinusoidal modulation with an average amplitude of 0.03 mag (Fig. 6). Given the possible magnetic nature of RX J0636 suggested by its spectroscopic appearance, we tentatively interpret these two signals as the white dwarf spin frequency (period) ω (P_{spin}) and an orbital sideband (beat) frequency $\omega \pm \Omega$, with Ω the orbital fre-
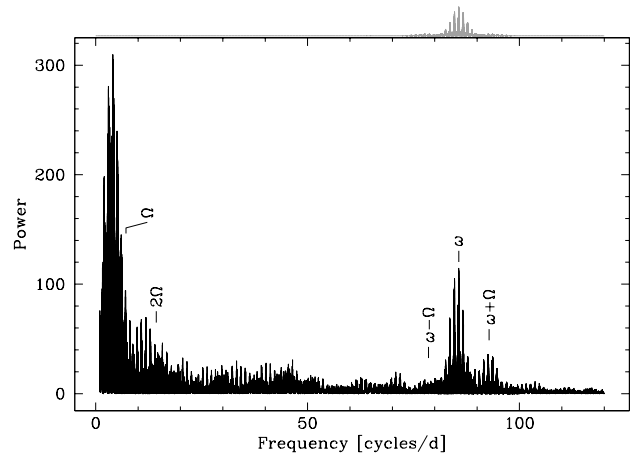
Figure 5. Scargle periodogram computed from the combined photometric data of RX J0636 (Table 1). We tentatively assign the peak detected at $85.7\,\mathrm{d}^{-1}$ (1008 s) to the white dwarf spin frequency ω and the peak at $92.9\,\mathrm{d}^{-1}$ (930 s) to the orbital side band $\omega + \Omega$. The location of the $\omega - \Omega$ side band is indicated. We caution, however, that the data does not allow an unambiguous identification, and that the true spin and side band signals may be swapped. No significant power is detected at the orbital period or its harmonic. The strong signal near $4\,\mathrm{d}^{-1}$ appears only in the 2005 data, and its nature is not clear. Shown on top of the Figure is the window function of the data set, shifted to ω.
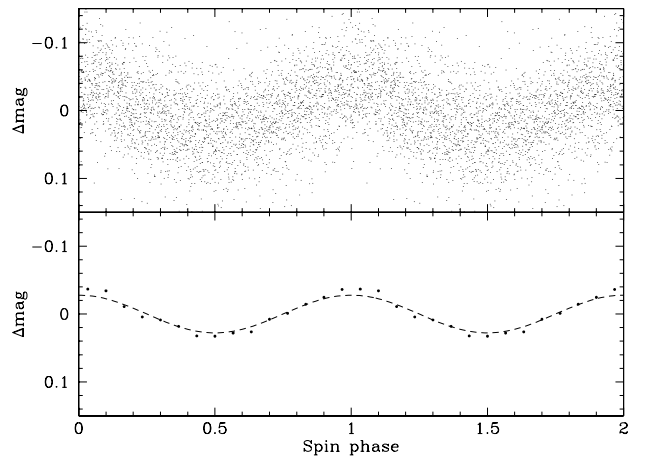
Figure 6. Spin-folded light curves of RX J0636, assuming $P_{\mathrm{spin}} = 1008.3408$ s. Top panel: all individual data points (Table 1). Variability on longer time scales has been removed from each individual night by subtracting the light curve smoothed by a 30-point box car. Bottom panel: Data binned into 30 phase slots. Plotted as dashed line is a sine fit to the binned & folded data.

quency, as the detection of these signals is the hallmark of the magnetic IPs. The optical photometry alone does not provide sufficient information to unambiguously identify the two signals, as both spin and beat dominated IPs are known. If the two photometric signals were indeed ω and $\omega \pm \Omega$, RX J0636 is expected to have an orbital period of $\simeq 201$ min. No significant power is detected in the periodogram near the corresponding frequency of $\simeq 7.15\,\mathrm{d}^{-1}$ (Fig. 5). Puzzling is the strong signal near $\simeq 4\,\mathrm{d}^{-1}$ ($\simeq 360$ min), which is detected in all the 2005 data, but absent in the 2004 data. The period of this photometric modulation is clearly much longer than the orbital period estimated from the beat period, and independently from
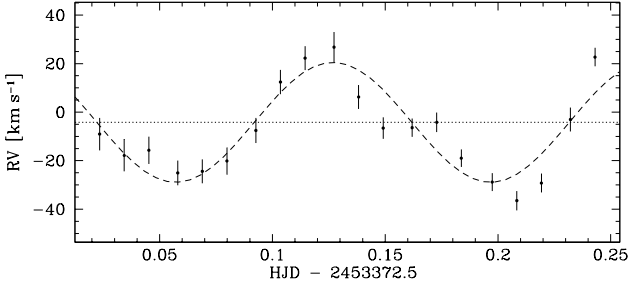
Figure 7. Radial velocity (RV) variation of Hα measured from the time-resolved WHT spectroscopy of RX J0636 (Table 1). Plotted as dashed line is a sine fit to the data, resulting in a period of 201(8) min. The dotted line indicates the systemic velocity determined from the sine fit, $\gamma = -4(2)\,\mathrm{km\,s^{-1}}$.

Table 4. HJD of the spin maxima (RX J0636, RX J0704, RX J1803) or spin minima (RX J1730), obtained from sine-fits to each individual night of photometric data.

System	HJD	System	HJD
RX J0636	2453299.564084	**RX J1730**	2452769.552687
	2453300.499631		2452780.528206
	2453301.491248		2452828.411952
	2453302.470448		2452829.411925
	2453423.366908		2452830.397171
	2453425.234453		2452830.397133
	2453426.214890		2452836.385213
	2453433.240185		2452837.395621
RX J0704	2453346.611013	**RX J1803**	2452781.436952
	2453372.526838		2452867.257081
	2453376.482737		2452868.260431
			2452869.245696
			2452870.248852
			2452871.252155

the time-resolved spectroscopy discussed below. Additional photometric observations will be necessary to confirm that this 360 min periodicity is a coherent and repeating characteristic of RX J1803.

5.1.2 Time-resolved spectroscopy

In order to test our hypothesis of RX J0636 being a CV with an orbital period near 201 min we have obtained 5.3 h time-resolved spectroscopy at the WHT (Table 1). Radial velocity measurements were carried out using a single Gaussian fit to Hα, the strongest emission line, fixing the full-width at half-maximum (FWHM) to $200\,\mathrm{km\,s^{-1}}$. The resulting radial velocity curve clearly shows a quasi-sinusoidal modulation with a amplitude of $\simeq 25\,\mathrm{km\,s^{-1}}$(Fig. 7). A Scargle periodogram computed from the radial velocity measurements shows a broad peak centred at $7.3\,\mathrm{d^{-1}}$, corresponding to 197 min. A sine fit to the radial velocities results in $P = 201(8)$ min, which is consistent with the orbital period estimate obtained from the photometry.

Based on the currently available spectroscopic and photometric observations, we consider RX J0636 a very likely IP candidate, with an orbital period of $P_{\mathrm{orb}} \simeq 201$ min and a white dwarf spin period of either $P_{\mathrm{spin}} = 1008.3048$ s or $P_{\mathrm{spin}} = 930.5829$ s.
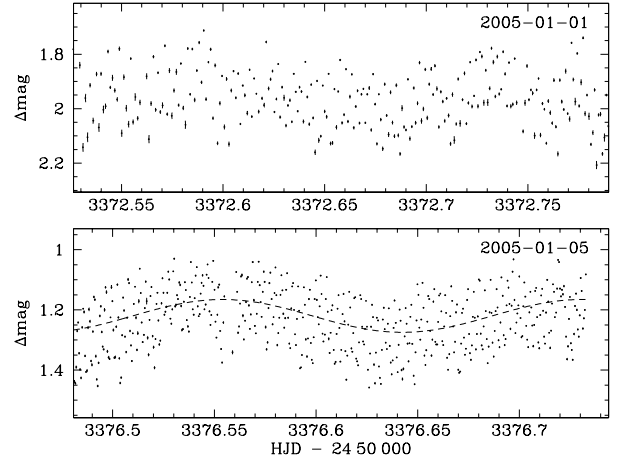
Figure 8. Sample light curves of RX J0704 obtained with the INT/WFC (top panel) and the TNG/DOLORES (bottom panel). The light curves are dominated by a modulation at twice the white dwarf spin period $P_{\mathrm{spin}} = 480.708$ s, and a longer-period modulation with $P \simeq 4$ h, which we tentatively identify as the orbital period. A sine fit to the TNG data gives $P_{\mathrm{orb}} = 254.7(1.1)$ min (dashed curve).
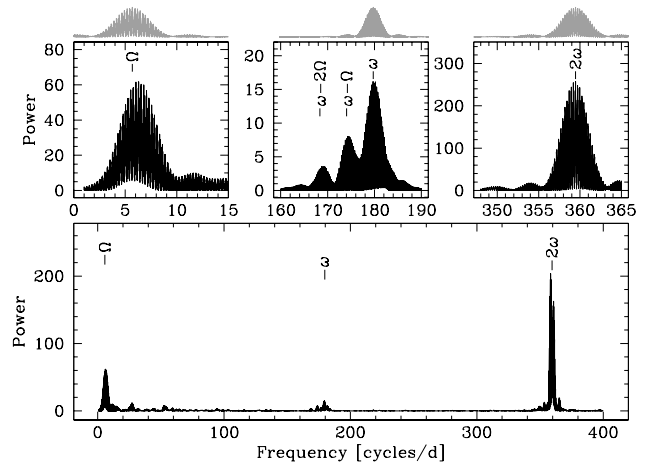

Figure 9. Scargle periodogram computed from the combined photometric data of RX J0704 (Table 1). Bottom panel: full frequency range. Middle panels, left to right: enlargement around the orbital, the white dwarf spin, and twice the white dwarf spin frequencies. Top panels: the window function calculated from the temporal sampling of the data, shifted to the assumed orbital (Ω), spin (ω), and first harmonic of the spin 2ω frequencies. The corresponding periods are $\simeq 250$ min, 480.708 s, and 240.354 s, respectively.

5.2 1RXS J070407.9+26250

The INT/IDS identification spectrum or RX J0704 (Fig. 2) is overall similar to that of RX J0636, with the difference of displaying somewhat broader lines. No signature of the secondary star is detected.

5.2.1 Photometry

The first brief photometric data set obtained at Kryoneri (Table 1) displayed substantial short-term variability with a peak-to-peak amplitude of ~ 0.3 mag. A Scargle periodogram computed from those data contained a strong signal at $\sim 360\,\mathrm{d^{-1}}$, identifying
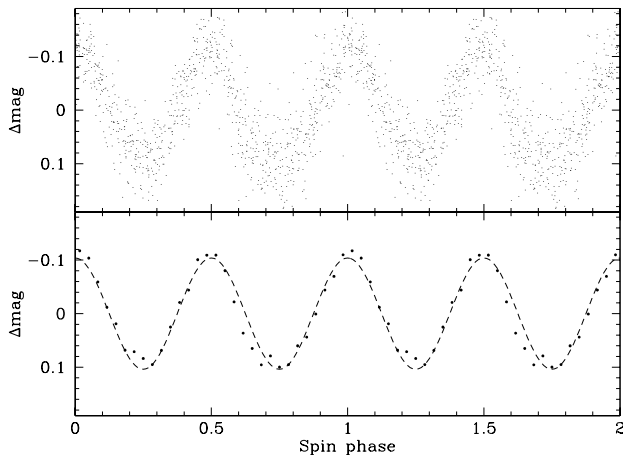
Figure 10. Spin-folded light curves of RX J0704 using $P_{\rm spin} = 480.708$ s. Top panel: all individual data points (Table 1). The putative orbital modulation has been removed prior to phase-folding by means of a 30-point boxcar. Bottom panel: Data binned into 30 phase slots. Plotted as dashed line is a sine fit to the binned & folded data.

RX J0704 as an IP candidate with a rather short white dwarf spin period. Figure 8 shows the more extensive photometry obtained at the INT and TNG (Table 1), which revealed a modulation with a period of ~ 4 h in addition to the spin variability. The strongest peak in a Scargle periodogram calculated from the entire data set is found at a period of 4 min (Fig. 9), consistent with the earlier Kryoneri result. However, the larger data set shows also power at 480 s, which we subsequently interpret as the white dwarf spin. The 240 s period is then the first harmonic of the spin, most likely due to the changing aspect of two accreting pole caps. The periodogram around $P_{\rm spin}$ and $2P_{\rm spin}$ is severely plagued by aliases, caused by the sparse data coverage over the base line of one month. The 240 s signal displays two nearly equally strong aliases, their periods determined from sine fits to the photometric data are 240.3540(22) s and 240.5329(22) s, and we adopt $P_{\rm spin} = 480.7080(44)$ s as the putative white dwarf spin. Table 4 lists the times of spin maxima for each night of photmetry, determined from fitting a sine-wave to the individual data sets (where the period was fixed to the value determined from the entire data set). As the two maxima per spin cycle are almost equal, there is the chance of a 0.5 cycle mismatch. We have detrended the ~ 4 h modulation from the photometric data by means of a 30-point boxcar, and show in Fig. 10 the detrended data folded over $P_{\rm spin}$. The spin light curve is quasi-sinusoidal with two nearly equal maxima per spin cycle, explaining the dominant power at $2P_{\rm spin}$. A sine fit to the folded data reveals some small differences in the pulse durations, which is the reason for the detection of power at the actual $P_{\rm spin}$.

The ~ 4 h modulation (especially conspicuous in the TNG light curve, Fig. 8 bottom panel), is reflected by the second strongest signal in the periodogram of the combined photometric data (Fig. 9). Formally this implies $P = 228.73(5)$ min, but the severe aliasing prevents a unique idenfication of the true period. A sine fit to the TNG data alone results in $P = 254.7(1.1)$ min. The close-up of the periodogram around the white dwarf spin frequency ω (Fig. 9, top middle panel) shows substantial power excess with respect to the window function in the form of two clusters of aliases at frequencies below ω. The separation between these signals and ω is $5.68\,{\rm d}^{-1}$ and $11.24\,{\rm d}^{-1}$. If interpreted as the beat frequencies $\omega - \Omega$ and $\omega - 2\Omega$, which are commonly detected in IPs, these sig-
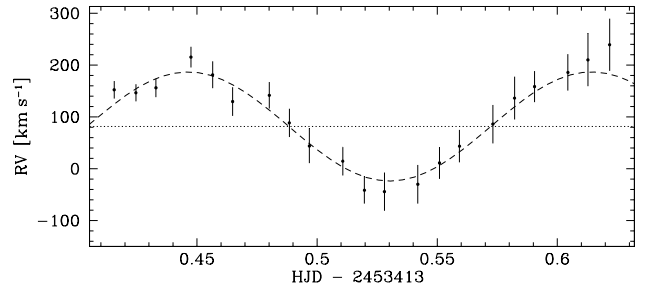
Figure 11. Radial velocity (RV) variation of Hα measured from the time-resolved Calar Alto spectroscopy of RX J0704 (Table 1). Plotted as dashed line is a sine fit to the data, resulting in a period of 242(7) min. The dotted line indicates the systemic velocity determined from the sine fit, $\gamma = 82(5)\,{\rm km\,s}^{-1}$.

nals imply an orbital period of $\simeq 250$ min. This falls well within the alias structure of the low-frequency signal, and is consistent with the period derived from the best (TNG) photometric data set.

5.2.2 *Time-resolved spectroscopy*

A single 5.6 h run of time-resolved spectroscopy of RX J0704 was obtained at Calar Alto in February 2005 (Table 1), with the aim to derive a dynamical estimate of the orbital period. The radial velocity variation of Hα was measured using a double Gaussian convolution (Schneider & Young 1980) with a separation of $1000\,{\rm km\,s}^{-1}$ and a FWHM of $400\,{\rm km\,s}^{-1}$. This Hα radial velocity curve displays a quasi-sinusoidal modulation with a semi-amplitude of $\simeq 110\,{\rm km\,s}^{-1}$(Fig. 11). The Scargle periodogram computed from these data contains a broad peak near $5.7\,{\rm d}^{-1}$ (253 min). Fitting a sine wave to the radial velocity data gives $P = 242(7)$ min, which agrees well with the period estimate derived from the TNG photometry.

We conclude on the base of the spectral, photometric, and X-ray properties of RX J0704 that this object is an IP with an orbital period of $\simeq 250$ min and a spin period of 480.708 s. The strong power at the first harmonic of the spin period suggests that both accreting poles contribute to a similar extent to the optical light.

5.3 **1RXS J173021.5-055933**

The identification of RX J1730 is the reddest of all four objects presented here, and displays the lowest emission line equivalent widths. Noticeable is the large equivalent width of He II λ 4686, which exceeds that of Hβ by a factor $\simeq 2$. The broad absorption feature near 5200 Å is an artifact from the data reduction that has been found in a number of other target stars.

5.3.1 *Photometry*

The JKT R-band photometry of RX J1730 obtained in May 2003 (Table 1) displayed short term variability with an amplitude of $\simeq 0.05$ mag, much in excess to the photometric errors of the individual data points. A Scargle periodogram computed from this data revealed strong signals near $675\,{\rm d}^{-1}$ and $1350\,{\rm d}^{-1}$. The latter frequency is undersampled by the data, resulting in a number of spurious downscattered signals. Prompted by this discovery, high-time resolution photometry of RX J1730 was obtained with the OGS in July 2003 (Table 1). Sample light curves of this run are show in Fig. 12. The periodogram computed from the OGS data displays
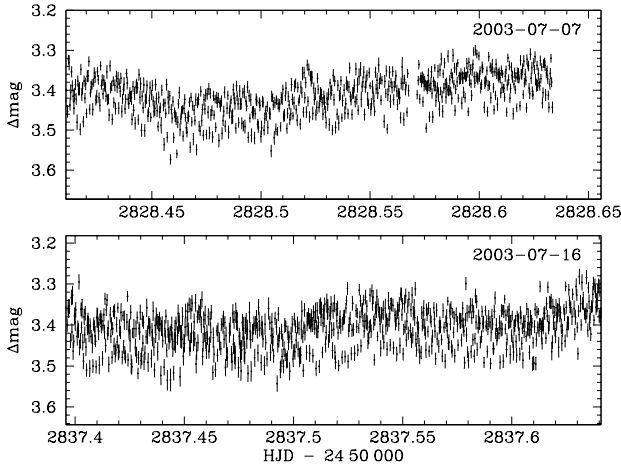
Figure 12. Sample filterless light curves of RX J1730 obtained with the 1 m OGS.
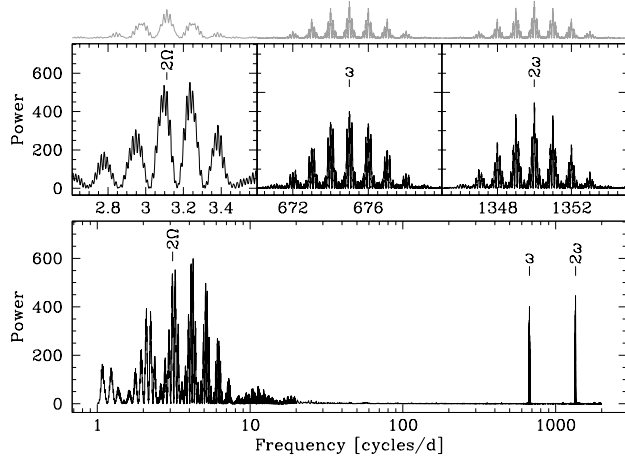
Figure 13. Scargle periodogram computed from the combined photometric data of RX J1730 (Table 1). Bottom panel: full frequency range, note the logarithmic frequency scale. Unambiguous signals are the white dwarf spin frequency at $\omega = 675 \, \mathrm{d}^{-1}$ ($P_{\mathrm{spin}} = 128 \, \mathrm{s}$). Orbital variability is detected at twice the orbital frequency ($P_{\mathrm{orb}} = 925.27 \, \mathrm{min}$), most likely reflecting the ellipsoidal modulation from the secondary star. Top panels, left to right: enlargement around the orbital, the white dwarf spin, and twice the white dwarf spin frequencies. Top panels: the window function calculated from the temporal sampling of the data, shifted to the assumed 2Ω, ω, and 2ω.

three distinct clusters of signals centred on $4.2 \, \mathrm{d}^{-1}$, $675 \, \mathrm{d}^{-1}$, and $1350 \, \mathrm{d}^{-1}$ (Fig. 13). The nature of the low-frequency signal will be discussed below together with the time-resolved spectroscopy.

The high-frequency signals unambiguously identify RX J1730 as an IP. We interpret the detection of the two commensurate signals as the white dwarf spin frequency and its first harmonic, suggesting that both poles contribute to the observed photometric modulation. Combining the OGS and JKT data, we determine $P_{\mathrm{spin}} = 127.999909(49) \, \mathrm{s}$. However, the two neighbouring aliases at $128.002689 \, \mathrm{s}$ and $127.997256 \, \mathrm{s}$ can not be excluded. Table 4 lists the times of spin minima (which can be unambiguously identified) for each night of photmetry, determined from fitting two sine-waves to the individual data sets (where the period was fixed to the value determined from the entire data set, but phases were left free for both sine waves). With a spin period of $128 \, \mathrm{s}$, RX J1730 is the
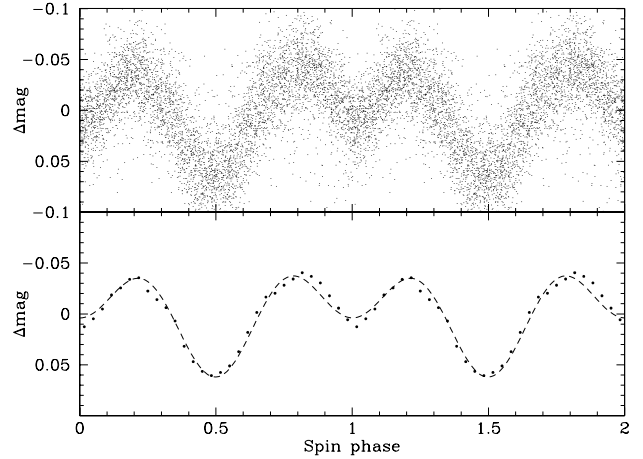
Figure 14. The photometric data of RX J1730 folded over the $128 \, \mathrm{s}$ spin period. Top panel: all individual data points. Bottom panel: data averaged into 30 phase bins. A two-frequency fit (ω and 2ω) is shown as dashed line.
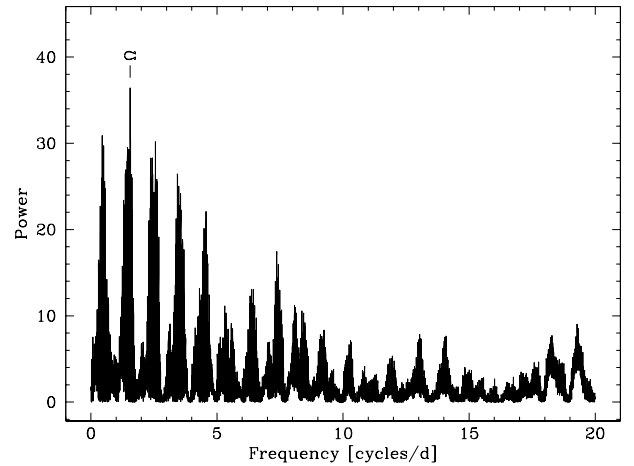
Figure 15. Scargle periodogram computed from the radial velocity variation of the He II λ 4686 line wings in RX J1730. The inferred orbital period is $P_{\mathrm{orb}} = 925.27 \, \mathrm{min}$.

second-fastest spinning white dwarf in an IP, behind by AE Aqr ($P_{\mathrm{spin}} = 33.08 \, \mathrm{s}$) and followed by DQ Her ($P_{\mathrm{spin}} = 140.1 \, \mathrm{s}$). The spin-folded light curve (Fig. 14) shows two maxima per spin cycle, with unequal minima. A two-frequency sine fit, with the higher frequency being fixed as the harmonic of the lower one, results in nearly equal amplitudes ($\simeq 0.03$) and a phase offset of ~ 0.57, suggesting nearly diametrically opposite pole caps on the white dwarf.

Comparing the amplitudes of the spin signal in the filered photometry obtained at the OGS in July 2003 (I: $0.03 \, \mathrm{mag}$, R: $0.035 \, \mathrm{mag}$, V: $0.057 \, \mathrm{mag}$) suggests that the spectrum of the 128 sec variabilty is blue, as expected for the emission from a hot pole cap. Additional data in B and U would be desirable to estimate a colour temperature for the spin modulation.

5.3.2 Time-resolved spectroscopy

The main purpose of obtaining time-resolved spectroscopy of RX J1730 was to determine the orbital period of the system. The first set of INT data (April 2003, Table 1) suggested a rather long period, prompting additional spectroscopic follow-up at the INT,

Figure 16. The He II λ4686 radial velocity (RV) measurements of RX J1730 folded over the orbital period of 925.27(14) min. Shown as a dashed line is a sine fit to the folded radial velocity data. The systemic velocity determined from the fit is $\gamma = 22(3)\,\mathrm{km\,s^{-1}}$.

Calar Alto, and Magellan. All spectra were binned on the dispersion of the lowest-resolution data (Calar Alto), corrected for the heliocentric velocity of the Earth, and continuum-normalised around Hα (not covered by the April 2003 data), Hβ and He II λ4686. Radial velocity measurements were carried out by means of correlating either a single Gaussian or a double Gaussian (Schneider & Young 1980), using a variety of widths (and separations in the case of the double Gaussian method). The radial velocity measurements were then subjected to a Scargle periodogram calculation. Whereas the analysis of the Ba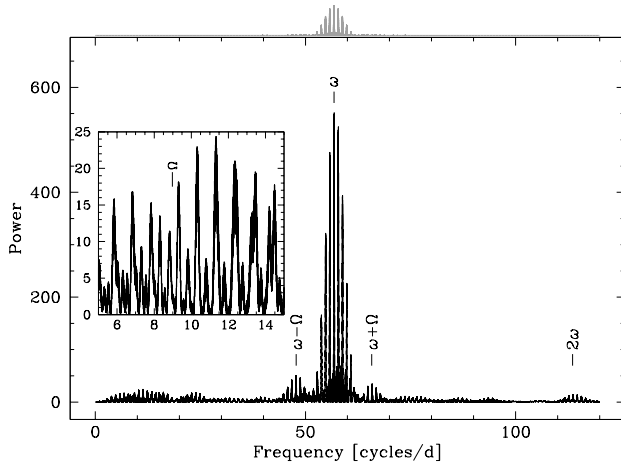lmer lines did not provide any conclusive result, the radial velocities measured from the He II λ4686 wings using a double-Gaussian convolution with a FWHM = 200 km s^{-1} and a separation of 1200 km s^{-1} yielded a well-defined signal at 1.556 d^{-1} in the periodogram (Fig. 15). A period of 925.27(14) min is derived from a sine fit to the He II radial velocity data, which we interpret as the orbital period of the system. Figure 16 shows the He II radial velocities folded over the orbital period. Inspecting the periodogram computed from the photometry (Fig. 13), it is apparent that twice the spectroscopic frequency coincides well with the one of the alias clusters in the low-frequency range, which suggests that ellipsoidal modulation is responsible for low-frequency photometric variability.

5.3.3 The Magellan average spectrum

Given the long orbital period of RX J1730, one might expect to detect its secondary star at optical wavelengths. In fact, a small contribution to the optical flux is suggested by the detection of ellipsoidal modulation in the photometric data. Figure 17 shows the average of the flux-calibrated spectra of RX J1730, which were obtained under very good atmospheric conditions. Whereas the majority of the strong absorption features are identified with diffuse interstellar bands (DIBs, Herbig 1995) or atomic interstellar absorption (Na I), weak absorption of Mg I λλ 5167,5172,5183 and the λλ4310 G-band are detected. Considering the strength of the DIBs, it is clear that the spectrum must be significantly reddened. For the galactic position of RX J1730 the dust maps by Schlegel et al. (1998) give an upper limit of $E(B-V) = 0.6$. An independent estimate is obtained using the neutral hydrogen maps of Dickey & Lockman (1990), which gives $N_\mathrm{H} = 1.66 \times 10^{21}\,\mathrm{cm^{-2}}$ for the line of sight towards RX J1730, corresponding to an upper limit of $E(B-V) = 0.34$ (Diplas & Savage 1994). For the following discussion, we will assume $E(B-V) = 0.45$. The weakness of the Mg I triplet and the G-band indicates that the secondary star contributes only a small fraction of the optical flux. In order to estimate the spectral type of the secondary star, we have taken mid-K to mid-

Figure 17. Bottom panel: the average of the Magellan spectra of RX J1730 obtained in June 2003. The major emission and absorption features are identified. The most noticeable features that are likely to be associated with the secondary star are the Mg I λλ 5167,5172,5183 triplet and the λ4310 G-band. All the strong absorption features are due to diffuse interstellar bands and interstellar sodium absorption. Middle panel: the average Magellan spectrum of RX J1730 along with a G6V star that has been reddened by $E(B-V) = 0.45$ and that contributes 15 % of the observed flux at 6800 Å. This main-sequence star spectrum approximately reproduces the strength of the observed stellar absorption features in RX J1730. The inset shows an enlarged view of the two spectra, demonstrating that a number of weak absorption lines are contained in both spectra. Top panel: the average Magellan spectrum dereddened by $E(B-V) = 0.45$, along with the (now unreddened) G6V star from the middle panel.

F star from the Jacoby et al. (1984) library, subjected them to an $E(B-V) = 0.45$ reddening, and then scaled them in flux to approximately match the strength of the Mg I triplet and the G-band absorption features observed in RX J1730. The absence of the broad λλ5000 − 5200 absorption band **[...does any of you know what this band is caused by?...]** excludes a spectral type later than ≃K0, and we find that spectral types in the range G4V to G0V, contributing ∼ 15% at 6800 Å, provide the best match for the observed line strengths (Fig. 17). From this exercise we conclude that the accretion flow is the dominant source of optical light in RX J1730.

We conclude that RX J1730 is an IP with an orbital period of 925.27 min and a white dwarf spin period of 128.0 s, which resembles in some aspects the enigmatic system AE Aqr. Differences are that its optical spectrum is dominated by the accretion flow and not by the secondary star, and that (so far) none of the flaring episodes characteristic of AE Aqr has been observed in RX J1730.

5.4   1RXS J180340.0+401214

The IDS identification spectrum of RX J1803 (Fig. 2) shows a typical CV spectrum with a negative Balmer decrement and relatively weak He II λ4686 emission, suggesting a possible magnetic nature of the system. Of all four CVs presented in this paper, RX J1803 has the lowest He II λ4686/Hβ flux ratio (Table 2).

**Figure 18.** Sample light curves of RX J1803 obtained at Kryoneri.

Figure 19. Scargle periodogram computed from the combined photometric data of RX J1803 (Table 1). Main panel: full frequency range. The orbital period and spin period are $P_{orb} = 160.21$ min and $P_{spin} = 1520.510$ s. Small panel: enlargement around the orbital frequency. Top panel: the window function calculated from the temporal sampling of the data, shifted to ω.

5.4.1 Photometry

The light curves of RX J1803 unmistakably reveal the presence of large-amplitude pulsations with a period of ~ 25 min (Fig. 18). The Scargle periodogram computed from the photometric data confirms the coherent nature of these pulsations (Fig. 19). A sine fit to the 5 consecutive nights of Kryoneri August 2003 data results in $P = 1520.510(66)$ s. The first harmonic of this signal is detected in the periodogram. Including the single night of data obtained with the JKT in May 2003 in the time series analysis results in substantial cycle count ambiguities due to the long separation from the August data, and does not improve the period determination. Power in excess of the alias structure is detected near $47.8\,d^{-1}$, and to a lesser degree near $65.9\,d^{-1}$. We interpret the strongest signal as the signature of the white dwarf rotation ω, and the two weaker symmetrically offset signals as orbital side bands, $\omega - \Omega$ and $\omega + \Omega$. Under this assumption, the orbital period of RX J1803 is $\simeq 159$ min, i.e. in the period gap. We note that no significant photometric variability at the orbital period is detected in the periodogram. The times of spin maxima for each night of photometry, determined from fitting
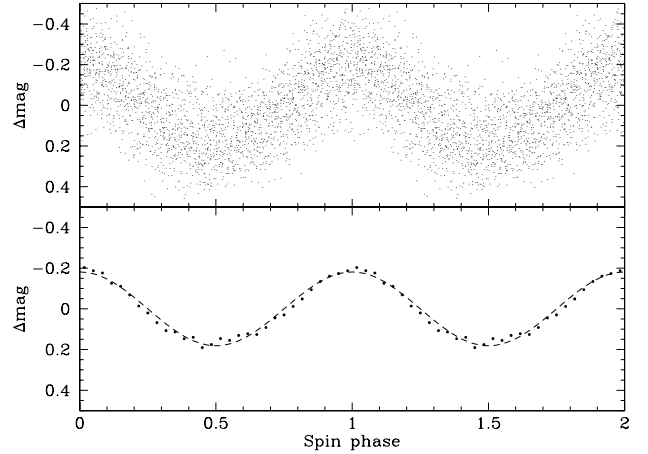
Figure 20. Spin-folded light curves of RX J1803, using $P_{spin} = 1520.510$ s. Top panel: all individual data points (Table 1). Bottom panel: Data binned into 30 phase slots. Plotted as a dashed line is a sine fit to the binned & folded data.
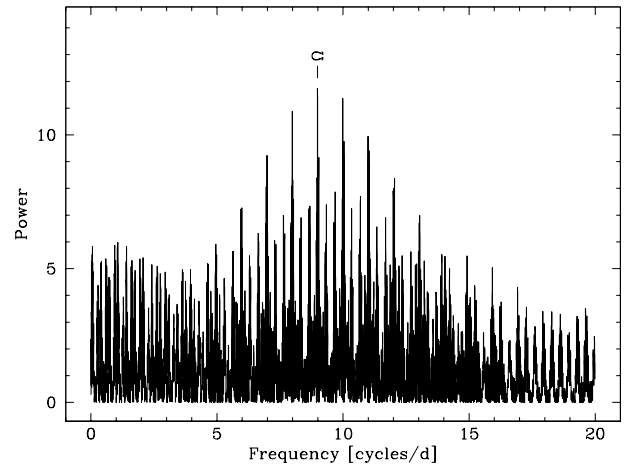
Figure 21. Scargle periodogram computed from the radial velocity variation of the Hα line wings in RX J1803, determining the orbital period to be $P_{orb} = 160.21$ min.
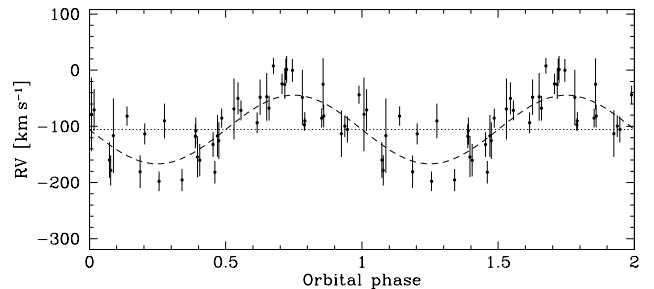
Figure 22. Radial velocities (RV) determined from the Hα wings in RX J1803, folded over the putative orbital period of 160.21(12) min. A sine fit to the folded radial velocities is shown as a dashed line. The systemic velocity determined from the fit is $\gamma = -100(7)\,km\,s^{-1}$.

a sine-wave to the individual data sets, are listed in Table 4 (where the period was fixed to the value determined from the entire data set).

5.4.2   Time-resolved spectroscopy

The time-resolved spectroscopy obtained at Calar Alto and at the INT (Table 1) provide the possibility for an independent orbital period determination. For this purpose, we have rebinned all spectra to a uniform wavelength scale, corrected for the heliocentric velocity of the Earth, and convolved the continuum-normalised profiles of Hα and He II λ 4686 with a double-Gaussian of fixed width (FWHM = 100 km s^{-1}) and separation 1400 km s^{-1}. A Scargle periodogram computed from the radial velocity measurements obtained in this way displays the strongest peak at $f \simeq 9.0\,\mathrm{d}^{-1}$(Fig. 21), flanked by 1-day aliases, which we interpret as the signature of the orbital frequency. A sine fit to the radial velocities results in $P_{\mathrm{orb}} = 160.21(12)$ min, which coincides with the orbital period estimated from the beat signals detected in the photometry. The Hα radial velocity data of RX J1803 folded over the orbital period is shown in Fig. 22.

In summary, RX J1803 is a bona-fide IP within the period gap, $P_{\mathrm{orb}} = 160.21$ min, and a likely white dwarf spin period of $P_{\mathrm{spin}} = 1520.510$ s.

6   DISCUSSION

We initiated a search for new CVs based on the X-ray/IR selection described in Sect. 2 with the aim to identify low-mass-transfer CVs close to the period minimum, such as WZ Sge, BW Scl, or GD 552, some of which might be period-bouncers. Our two identification runs led to the discovery of 12 new CVs, representing an impressive "hit-rate" of 7 %, but *none* of the newly identified systems resembles the short-period template systems. Wheras these three template systems have RASS count rates and *B*-band magnitudes comparable to the (WZ Sge: 0.2 cts s^{-1}, $B = 15.2$; BW Scl: 0.18 cts s^{-1}, $B = 15.6$, GD 552: 0.18 cts s^{-1}, $B = 16.6$), it may be that these three systems are *not* typical representatives of short-period low-mass-transfer CVs, and may exhibit by a higher X-ray emission. Moreover, the optical flux of low-mass-transfer CVs is dominated by the emission of the white dwarf. For an assumed white dwarf temperature of 15 000 K, our brightness cut-off of $R = 17$ corresponds to a maximum distance of $\simeq 125$ pc. While this white dwarf temperature is appropriate for WZ Sge, it may well be that the bulk of the short-period CVs have cooler white dwarfs, for a white dwarf temperature of 10 000 K $R = 17$ corresponds to a maximum distance of ~ 85 pc only. The conclusion from our survey at its current state is that there is not a large population of quiescent nearby WZ Sge-like stars, and that a large population of low-mass-transfer CVs can only exist if they look different from WZ Sge and look-alikes. One example of a "true" low-mass-transfer CV is the recently identified HS 2331+3905, which contains indeed a cool ($\simeq 10\,000$ K) white dwarf and is not detected in the RASS, although it is at a nearby distance of $\simeq 90$ pc (Araujo-Betancor et al. 2005).

A large fraction (two thirds) of the new CVs displays moderate to strong He II λ 4686 emission, suggestive of a magnetic nature – not too surprising, as $\sim 60\%$ of all X-ray discovered CVs are either polars or IPs (Gänsicke 2004). What is surprising, however, is the very large fraction (one third) of new IPs identified in this sample.
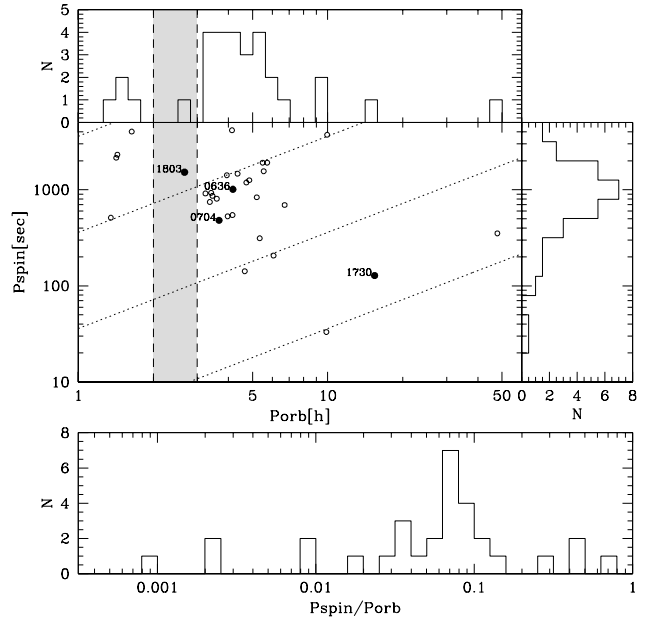
Figure 23. Centre panel: Orbital and spin periods of 31 confirmed IPs. The dotted lines indicate (from top to bottom) $P_{\mathrm{spin}}/P_{\mathrm{orb}} = 1, 0.1, 0.01, 0.001$. Top panel: Orbital period distribution of the known IPs, the $2-3$ h period gap is shaded gray. Right panel: Spin period distribution of the known IPs. The four new systems presented in this paper are shown as filled symbols.

6.1   Intermediate polars: A growing family

The census of IPs is probably the worst defined of all CV subclasses. The IP page by K. Mukai[2] lists 25 confirmed IPs. The latest edition (7.4) of Ritter & Kolb (2003) has 37 IPs, and Downes et al. (2001) contains 46 IPs. The defining criterion of an IP is the detection of *coherent* short-period variability over a sufficiently long period of time, that can be associated with the white dwarf spin – and it is the differing degrees of strictness in applying this criterion which causes the large disagreement in the head count of IPs. We adopted Mukai's conservative classification, and updated his list by RX J0153.3+7446 ($P_{\mathrm{spin}} = 1414$ s, Haberl & Motch 1995; $P_{\mathrm{orb}} = 236.48$ min, Thorstensen, priv.comm.) and HS0943+1404 ($P_{\mathrm{spin}} = 4150$ s, $P_{\mathrm{orb}} \simeq 250$ min, Rodríguez-Gil et al. 2005), as well as the four new IPs presented here, the current roster of IPs encompasses 31 systems[3].

Figure 23 shows the distribution of these 31 systems in the $P_{\mathrm{orb}} - P_{\mathrm{spin}}$ plane, their orbital and spin period distributions, as well as the distribution in $P_{\mathrm{spin}}/P_{\mathrm{orb}}$. A large fraction of all IPs is found near $P_{\mathrm{spin}}/P_{\mathrm{orb}} \simeq 0.1$, which was first noticed by Barrett et al. (1988), and stimulated theoretical work on the white dwarf spin equilibrium in magnetic CVs (King & Lasota 1991; Warner & Wickramasinghe 1991). Later, King & Wynn (1999) showed that

[3] Thus, our definition of IPs excludes systems showing coherent variability at extremely short periods that lack the definite evidence of these periods being related to the white dwarf spin (e.g. WZ Sge; Robinson et al. 1978 and HS2331+3905; Araujo-Betancor et al. 2005), nearly-synchronous polars, systems such as V795 Her or LS Peg, i.e. members of the SW Sex class which might contain a magnetic white dwarf (Rodríguez-Gil et al. 2001) but which lack undisputable measurements of P_{spin}, and systems for which the presence of coherent variability is supported only by moderately small amounts of data.

spin equilibria with $P_{\rm spin}/P_{\rm orb} > 0.1$ exist, explaining systems such as EX Hya. Based on their calculations, King & Wynn (1999) predicted that most IPs with $P_{\rm spin}/P_{\rm orb} > 0.1$ should have orbital periods below the period gap – which agrees with Fig. 23. Most recently, Norton et al. (2004) found that a large range of spin equilibria exists in the $(P_{\rm spin}/P_{\rm orb}, \mu_{\rm wd}, P_{\rm orb})$ parameter space, where $\mu_{\rm wd}$ is the magnetic moment of the white dwarf. Assuming that the majority of the observed IPs are close to their spin equilibria, Norton et al. (2004) estimated their $\mu_{\rm wd}$ from the model calculations. Using their Fig. 2, we estimate the magnetic moments of the white dwarfs in RX J0636, RX J0704, and RX J1803 to be $\sim 3 \times 10^{33}\,\mathrm{G\,cm}^3$, $\sim 1 \times 10^{33}\,\mathrm{G\,cm}^3$, and $\sim 4 \times 10^{33}\,\mathrm{G\,cm}^3$, respectively. In that respect, RX J0636 and RX J1803 are similar to the bulk of the previously known IPs, whereas RX J0704 resembles V405 Aur or YY Dra.

The case of RX J1730 is quite different, its very low $P_{\rm spin}/P_{\rm orb}$ and long orbital period suggests that the white dwarf is rotating much faster than its equilibrium spin period, and we suggest that it is similar to AE Aqr. In AE Aqr, the rapid white dwarf spin is actually preventing accretion onto the white dwarf (Wynn et al. 1997), and the mass-ejection from the system explains the large observed spin-down rate of the white dwarf (de Jager et al. 1994). Schenker et al. (2002) suggested that AE Aqr descended from a supersoft X-ray binary which only recently ($\sim 10^7$ yr ago) turned from a phase of extremely high (thermal-timescale) mass transfer into a (not quite) "ordinary" CV. AE Aqr differs from normal CVs in having a spectral type which is too late for its orbital period, and an extreme N/C overabundance. Gänsicke et al. (2003) have shown that a substantial fraction of CVs ($\sim 10 - 15\%$) show evidence for enhanced N/C abundances, confirming that thermal-time scale mass transfer may represent an important CV formation channel. If RX J1730 is indeed a sibling of AE Aqr, we predict that it should show a measurable spin-down of the white dwarf rotation, and is likely to exhibit an enhanced N/C abundance ratio as well. It may also show the flaring characteristic of AE Aqr.

The class of IPs has seen a substantial growth in number over the last few years, and more than 20 % of all confirmed IPs were identified by us, DW Cnc (= HS 0756+1624, literally a twin of V1025 Cen, Rodríguez-Gil et al. 2004, see also Patterson et al. 2004), 1RXS J062518.2+733433 (= HS 0618+7336, a "standard" IP, Araujo-Betancor et al. 2003), and HS 0943+1404 (an IP with long $P_{\rm orb}$ and small $P_{\rm spin}/P_{\rm orb}$, Rodríguez-Gil et al. 2005) as part of our search for CVs in the Hamburg Quasar Survey, and RX J0636, RX J0704, RX J1730 and RX J1803 in the ROSAT/2MASS selected CV sample described in this paper. These seven new IPs span a large range in orbital and spin periods, with $0.0023 < P_{\rm spin}/P_{\rm orb} < 0.43$, demonstrating rich variety of systems among the newly identified CVs.

6.2 INTEGRAL – a bloodhound for hunting down IPs?

RXJ 1730 has been detected as a significant INTEGRAL source (IGR J17303–0601, $0.28 \pm 0.03\,\mathrm{cts\,s}^{-1}$) in the IBIS/ISGRI soft gamma ray galactic plane survey (GPS) (Bird et al. 2004). Masetti et al. (2004) observed three optically unidentified INTEGRAL sources, including RX J1730. Based on their single spectrum of RX J1730, which is similar to our data shown in Fig. 2, the authors suggested that the object is a low-mass X-ray binary in the Galactic bulge. However, the detection of a 128 s spin period in our optical photometry clearly identifies RX J1730 as an IP. Inspecting the IBIS GPS catalogue (Bird et al. 2004), 6 out of the 123 sources are CVs, of which four are IPs (1RXS J154814.5-

Table 5. Orbital and spin periods of the four new IPs.

System	$P_{\rm orb}$ [min]	$P_{\rm spin}$ [s]
RX J0636	$\simeq 201$	1008.3408(19) or 930.5829(40)
RX J0704	$\simeq 250$	480.7080(44)
RX J1730	925.27(14)	127.999909(49)
RX J1803	160.21(12)	1520.510(66)

452845, V2400 Oph, RX J1730, and V1223 Sgr), one is an asynchronous polar (V1432 Aql) and one is a (non-magnetic) dwarf nova (SS Cyg). Whereas the dominant population of ROSAT-discovered CVs were X-ray soft polars, the harder X-ray spectrum of IPs makes them the most prolific CV type contained in X-ray surveys of the Galactic plane, where interstellar absorption will suppress the X-ray soft polars even for relatively short distances. It appears that optical follow-up of unidentified INTEGRAL GPS sources may turn out to be a significant discovery chanel for IPs.

7 CONCLUSIONS

We have initiated a search for CVs selecting targets from the ROSAT Bright Source catalogue and discriminating against AGN by using a 2MASS infrared colour-cut. Whereas our aim was to find members of the "missing" population of low-mass-transfer CVs near the minimum period, we predominantly discovered new magnetic CVs, among which are four IPs: RX J0636, RX J0704, RX J1730, and RX J1803. RX J0636 ($P_{\rm orb} \simeq 201$ min, $P_{\rm spin} = 1008.3408$ s or 930.5829 s) and RX J1803 ($P_{\rm orb} = 160.21$ min, $P_{\rm spin} = 1520.510$ s) are rather typical IPs, except for RX J1803 being the first confirmed IP in the period gap. RX J0704 ($P_{\rm orb} \simeq 250$ min, $P_{\rm spin} = 480.708$ s) appears to be similar to V405 Aur or YY Dra. The most striking new CV is RX J1730 ($P_{\rm orb} = 925.27$ min, $P_{\rm spin} = 128.0$ s), which may be a sibling of AE Aqr. RX J1730 is also a moderately bright hard X-ray source in the INTEGRAL/IBIS Galactic plane survey.

REFERENCES

Abbott, T. M. C., Fleming, T. A., & Pasquini, L. 1997, A&A, 318, 134

Araujo-Betancor, S., Gänsicke, B. T., Hagen, H.-J., et al. 2005, A&A, 430, 629

Araujo-Betancor, S., Gänsicke, B. T., Hagen, H.-J., Rodríguez-Gil, P., & Engels, D. 2003, A&A, 406, 213

Barrett, P., O'Donoghue, D., & Warner, B. 1988, MNRAS, 233, 759

Bertin, E. & Arnouts, S. 1996, A&AS, 117, 393

Bird, A. J., Barlow, E. J., Bassani, L., et al. 2004, ApJ Lett., 607, L33

de Jager, O. C., Meintjes, P. J., O'Donoghue, D., & Robinson, E. L. 1994, MNRAS, 267, 577

Dickey, J. M. & Lockman, F. J. 1990, ARA&A, 28, 215

Diplas, A. & Savage, B. D. 1994, ApJ, 427, 274

Downes, R. A., Webbink, R. F., Shara, M. M., et al. 2001, PASP, 113, 764

Gänsicke, B. T. 2004, in The Astrophysics of Cataclysmic Variables and Related Objects, ed. J.-M. Hameury & J.-P. Lasota (ASP Conf. Ser. in press)

Gänsicke, B. T., Araujo-Betancor, S., Hagen, H.-J., et al. 2004, A&A, 418, 265

Gänsicke, B. T., Beuermann, K., & Reinsch, K., eds. 2002a, The Physics of Cataclysmic Variables and Related Objects (ASP Conf. Ser. 261)

Gänsicke, B. T., Hagen, H. J., & Engels, D. 2002b, in The Physics of Cataclysmic Variables and Related Objects, ed. B. T. Gänsicke, K. Beuermann, & K. Reinsch (ASP Conf. Ser. 261), 190–199

Gänsicke, B. T., Szkody, P., de Martino, D., et al. 2003, ApJ, 594, 443

Haberl, F. & Motch, C. 1995, A&A, 297, L37

Herbig, G. H. 1995, ARA&A, 33, 19

Howell, S. B., Rappaport, S., & Politano, M. 1997, MNRAS, 287, 929

Jacoby, G. H., Hunter, D. A., & Christian, C. A. 1984, ApJS, 56, 257

King, A. R. & Lasota, J. P. 1991, ApJ, 378, 674

King, A. R. & Wynn, G. A. 1999, MNRAS, 310, 203

Kolb, U. 1993, A&A, 271, 149

Kolb, U. & Stehle, R. 1996, MNRAS, 282, 1454

Marsh, T. R., Morales-Rueda, L., Steeghs, D., et al. 2002, in The Physics of Cataclysmic Variables and Related Objects, ed. B. T. Gänsicke, K. Beuermann, & K. Reinsch (ASP Conf. Ser. 261), 200–207

Masetti, N., Palazzi, E., Bassani, L., Malizia, A., & Stephen, J. B. 2004, A&A, 426, L41

Meyer-Hofmeister, E., Meyer, F., & Liu, B. F. 1998, A&A, 339, 507

Monet, D. G., Levine, S. E., Canzian, B., et al. 2003, AJ, 125, 984

Norton, A. J., Wynn, G. A., & Somerscales, R. V. 2004, ApJ, 614, 349

Paczyński, B. & Sienkiewicz, R. 1983, ApJ, 268, 825

Patterson, J., Thorstensen, J. R., Vanmunster, T., et al. 2004, PASP, 116, 516

Rappaport, S., Joss, P. C., & Verbunt, F. 1983, ApJ, 275, 713

Ritter, H. & Kolb, U. 2003, A&A, 404, 301

Robinson, E. L., Nather, R. E., & Patterson, J. 1978, ApJ, 219, 168

Rodríguez-Gil, P., Casares, J., Martínez-Pais, I. G., Hakala, P., & Steeghs, D. 2001, ApJ Lett., 548, L49

Rodríguez-Gil, P., Gänsicke, B. T., Araujo-Betancor, S., & Casares, J. 2004, MNRAS, 349, 367

Rodríguez-Gil, P., Gänsicke, B. T., Hagen, H.-J., et al. 2005, A&A, submitted

Scargle, J. D. 1982, ApJ, 263, 835

Schenker, K., King, A. R., Kolb, U., Wynn, G. A., & Zhang, Z. 2002, MNRAS, 337, 1105

Schlegel, D. J., Finkbeiner, D. P., & Davis, M. 1998, ApJ, 500, 525

Schneider, D. P. & Young, P. 1980, ApJ, 238, 946

Schwope, A. D., Hambaryan, V., Schwarz, R., Kanbach, G., & Gänsicke, B. T. 2002, A&A, 392, 541

Szkody, P., Henden, A., Fraser, O., et al. 2005, AJ, in press

Voges, W., Aschenbach, B., Boller, T., et al. 1999, A&A, 349, 389

Warner, B. 1987, MNRAS, 227, 23

Warner, B. & Wickramasinghe, D. T. 1991, MNRAS, 248, 370

Wynn, G. A., King, A. R., & Horne, K. 1997, MNRAS, 286, 436

This paper has been typeset from a TEX/ LATEX file prepared by the author.